



Diverse Carbonates in Exoplanet Oceans Promote the Carbon Cycle

Kaustubh Hakim¹ , Meng Tian¹ , Dan J. Bower¹ , and Kevin Heng^{2,3,4} ¹ Center for Space and Habitability, University of Bern, Gesellschaftsstrasse 6, CH-3012 Bern, Switzerland; kaustubh.hakim@unibe.ch² Ludwig Maximilian University, University Observatory Munich Scheinerstrasse 1, Munich D-81679, Germany³ Department of Physics, Astronomy & Astrophysics Group, University of Warwick, Coventry, CV4 7AL, UK⁴ ARTORG Center for Biomedical Engineering Research, University of Bern, Murtenstrasse 50, CH-3008, Bern, Switzerland

Received 2022 September 4; revised 2022 November 30; accepted 2022 December 5; published 2023 January 5

Abstract

Carbonate precipitation in oceans is essential for the carbonate-silicate cycle (inorganic carbon cycle) to maintain temperate climates. By considering the thermodynamics of carbonate chemistry, we demonstrate that the ocean pH decreases by approximately 0.5 for a factor of 10 increase in the atmospheric carbon dioxide content. The upper and lower limits of ocean pH are within 1–4 of each other, where the upper limit is buffered by carbonate precipitation and defines the ocean pH when the carbon cycle operates. If the carbonate compensation depth (CCD) resides above the ocean floor, then carbonate precipitation and the carbon cycle cease to operate. The CCD is deep (>40 km) for high ocean temperature and high atmospheric carbon dioxide content. Key divalent carbonates of magnesium, calcium and iron produce an increasingly wider parameter space of deep CCDs, suggesting that chemical diversity promotes the carbon cycle. The search for life from exoplanets will benefit by including chemically more diverse targets than Earth twins.

Unified Astronomy Thesaurus concepts: Extrasolar rocky planets (511); Carbon dioxide (196); Habitable zone (696); Ocean-atmosphere interactions (1150); Geological processes (2288)

1. Introduction

The carbonate-silicate cycle, also known as the inorganic carbon cycle, is a negative climate feedback mechanism that stabilizes the surface temperature via the greenhouse effect of carbon dioxide in response to changes in volcanism rates, stellar luminosity, atmospheric composition and opacity, planetary orbital movements, and spin axis tilt (Berner 2004; Catling & Kasting 2017). Continental silicate rocks and atmospheric carbon dioxide react with water in a process known as silicate weathering to produce carbonate-forming ions that precipitate as carbonates onto the ocean floor (Walker et al. 1981). The carbon cycle is completed when carbonates are transferred into the mantle for deep storage or carbon is eventually released back into the atmosphere by volcanism (Holland 1978; Sleep & Zahnle 2001), although the degassing efficiency is debated (Foley 2015; Kelemen & Manning 2015). Silicate weathering and carbonate precipitation are traditionally represented by the net chemical reaction (Walker et al. 1981)



where wollastonite (CaSiO_3), which serves as a proxy for silicate rocks, is converted into calcite (CaCO_3). Calcium thus plays a crucial role in silicate weathering and carbonate precipitation and is present as Ca^{2+} cations in oceans (Section 2).

The existence of habitable zones assumes that the carbon cycle operates on Earth analogs to stabilize their atmospheric carbon dioxide content (Kasting et al. 1993). Implicitly, this assumes not only that silicate weathering operates, but that ocean floor precipitation and deep storage of carbonates also occur. There exists a critical ocean depth known as the

carbonate compensation depth (CCD), below which carbonates are unable to exist in their solid form because carbonate solubility increases with pressure in the ocean (Zeebe & Westbroek 2003; see also Section 2.3, Figure 1). In modern Earth oceans, the CCD is located between 4 and 5 km, below the average ocean depth of about 3.8 km (Zeebe 2012). If the CCD resides at a depth above the ocean floor, then carbonates are unable to settle. This leads to the disruption of the carbon cycle—at least, as it is understood to operate on Earth. Moreover, there are currently no theoretical constraints on exoplanet ocean chemistry. We investigate the interplay between atmospheric carbon dioxide content, ocean acidity (pH), and carbonate precipitation. We then calculate the CCD over a broad range of physical conditions.

2. Methods

2.1. Ocean Chemistry Model

2.1.1. Calcium System

Ocean chemistry is modeled by considering thermochemical equilibrium for pure calcium, magnesium, or iron systems. The CO_2 partial pressure P_{CO_2} , ocean–surface temperature T , and local ocean pressure P_{oc} are control parameters (Figure 1, Table 1). In the Ca system, there are 13 unknowns, the number density n of H^+ , OH^- , H_2O , HCO_3^- , CO_3^{2-} , $\text{CO}_2(\text{aq})$, Ca_{tot} , Ca^{2+} , $\text{SiO}_{2,\text{tot}}$, $\text{SiO}_2(\text{aq})$, quartz $\text{SiO}_2(\text{s})$, wollastonite $\text{CaSiO}_3(\text{s})$ and calcite $\text{CaCO}_3(\text{s})$. Out of the 13 unknowns, two are continental silicate weathering products, $n_{\text{Ca}_{\text{tot}}}$ and $n_{\text{SiO}_{2,\text{tot}}}$, that depend on P_{CO_2} and T (Section 2.2). There are 11 remaining unknowns. We solve for three mass-conservation equations (for H, Ca, and SiO_2), one charge balance equation, and seven equations from seven chemical reactions providing relations between equilibrium constants (that depend on P_{oc} and T), reactants and products.

These three mass-conservation equations, one charge balance equation and seven reactions (water dissociation,

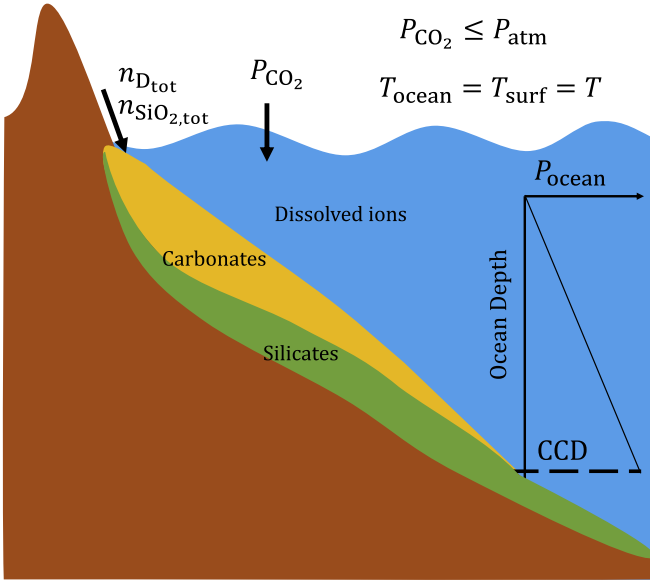
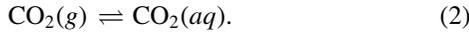


Figure 1. Model parameters, $n_{D_{\text{tot}}}$, where $D = \text{Ca, Mg or Fe}$, $n_{\text{SiO}_2, \text{tot}}$, P_{CO_2} , P_{atm} , P_{oc} , and T . See Section 2 and Table 1 for a full list of output quantities and description.

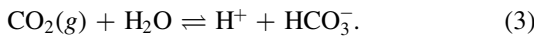
Table 1
Parameters and output quantities

Symbol	Description	Reference
<i>Parameters for ocean chemistry</i>		
T	Ocean–surface temperature	288 K
P_{CO_2}	CO_2 partial pressure	0.3 mbar
P_{atm}	Atmospheric pressure	1 bar
P_{oc}	Ocean layer pressure	1 bar
<i>Parameters for weathering</i>		
$n_{D_{\text{tot},0}}$	Ca, Mg or Fe ref. number density	1 m^{-3}
β	Weathering power-law exponent	0.3
T_e	e -folding temperature	13.7 K
<i>Output quantities</i>		
n_X	Number density of X (m^{-3})	
pH	$-\log_{10}(n_{\text{H}^+}/n_0)$; $n_0 = 10^3 \text{ m}^{-3}$	

Henry’s law/physical CO_2 dissolution, chemical CO_2 dissolution, bicarbonate ion dissociation, calcite precipitation, quartz precipitation and wollastonite precipitation) are specified below. Henry’s law gives the amount of CO_2 physically dissolved in ocean water in equilibrium with P_{CO_2} :



The chemical dissolution or dissociation of CO_2 in ocean water leads to the production of HCO_3^- and H^+ ions and thereby increases the ocean acidity (and decreases ocean $\text{pH} = -\log_{10}(n_{\text{H}^+}/n_0)$, where the standard number density $n_0 = 1 \text{ m}^{-3}$) by the following reaction:

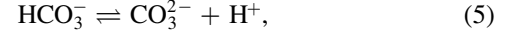


To maintain the charge balance in ocean water, the addition of Ca^{2+} to oceans decreases the number density of H^+ and hence increases the ocean pH. The charge balance equation is given

by

$$2n_{\text{Ca}^{2+}} + n_{\text{H}^+} = n_{\text{HCO}_3^-} + 2n_{\text{CO}_3^{2-}} + n_{\text{OH}^-}, \quad (4)$$

where CO_3^{2-} is produced due to the bicarbonate dissociation reaction:



and where OH^- is produced due to the water dissociation reaction:



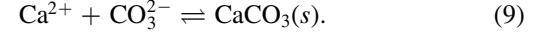
The mass conservation of H is given by

$$n_{\text{H}_{\text{tot}}} = 2n_{\text{H}_2\text{O}} + n_{\text{H}^+} + n_{\text{HCO}_3^-}. \quad (7)$$

Ca_{tot} partitions into Ca^{2+} , calcite, and wollastonite, which is accounted for by mass conservation:

$$n_{\text{Ca}_{\text{tot}}} = n_{\text{Ca}^{2+}} + n_{\text{Cal}} + n_{\text{Wo}}. \quad (8)$$

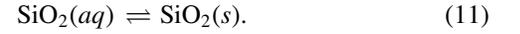
Calcite precipitation occurs when $n_{\text{Ca}^{2+}}$ is saturated to a certain value determined by the equilibrium constant of the calcite precipitation reaction and the abundance of $n_{\text{CO}_3^{2-}}$:



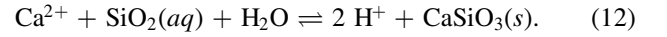
SiO_2, tot partitions into aqueous silica $\text{SiO}_2(\text{aq})$, quartz $\text{SiO}_2(\text{s})$, and wollastonite $\text{CaSiO}_3(\text{s})$. The mass conservation for SiO_2 is given by

$$n_{\text{SiO}_2, \text{tot}} = n_{\text{SiO}_2(\text{aq})} + n_{\text{Qz}} + n_{\text{Wo}}. \quad (10)$$

The quartz precipitation reaction is



The reaction of wollastonite precipitation is given by



These equilibrium chemistry calculations are performed using `Reaktoro v2` (Leal 2015), a multiphase (aqueous, gas, and solid mineral phases) chemistry software. This software implements the extended law of mass action including the determination of stable and unstable species for a given set of species in the system (Leal et al. 2017). We use the SUPCRTBL database for thermodynamic data (Johnson et al. 1992; Zimmer et al. 2016), the Peng–Robinson activity model for gases (Peng & Robinson 1976), the Helgeson–Kirkham–Flowers activity model for water (Helgeson et al. 1981), and the Drummond activity model for $\text{CO}_2(\text{aq})$ (Drummond 1981).

2.1.2. Magnesium and Iron Systems

In the Mg system, Ca is replaced by Mg, calcite by magnesite $\text{MgCO}_3(\text{s})$, and wollastonite by enstatite $\text{Mg}_2\text{Si}_2\text{O}_6(\text{s})$. This includes replacing equilibrium constants of all reactions including Mg. Similarly, in the Fe system, Ca is replaced by Fe, calcite by siderite $\text{FeCO}_3(\text{s})$, and wollastonite by fayalite $\text{Fe}_2\text{SiO}_4(\text{s})$. We limit our calculations to Fe^{2+} although its oxidation has inhibited the formation of siderite during Earth’s history, particularly since the Great Oxidation Event (Rye et al. 1995).

2.2. Weathering Model

The introduction of carbonate-producing divalent cations in oceans is dictated by silicate weathering. Silicate weathering and therefore the total number density of divalent cations D^{2+}

(D = Ca, Mg or Fe) must depend on the CO_2 partial pressure P_{CO_2} and surface temperature T (Walker et al. 1981; Hakim et al. 2021),

$$n_{\text{D}_{\text{tot}}} = f_W(P_{\text{CO}_2}, T) = n_{\text{D}_{\text{tot},0}} \left(\frac{P_{\text{CO}_2}}{P_{\text{CO}_2,0}} \right)^\beta \exp\left(\frac{T - T_0}{T_e}\right), \quad (13)$$

where “0” represents the Earth reference values (Table 1), $T_e = 13.7$ K is the e -folding temperature, and $\beta = 0.3$ is the weathering power-law exponent (Walker et al. 1981). However, not all added Ca (or Mg, Fe) in oceans remains in the form of divalent cations: a fraction of it precipitates as carbonates on the ocean floor and another fraction as silicates. For this reason, we perform partitioning calculations of Ca (or Mg, Fe) in different phases following the ocean chemistry model (Section 2.1).

2.3. Carbonate Compensation Depth Model

Carbonates are deposited onto the ocean floor as part of sediments. The transition from calcite-rich to calcite-free sediments is gradual. The CCD for the Earth’s oceans is normally defined as the depth at which the dissolution flux of calcite balances the precipitation flux (Zeebe 2012). The depth at which the rapid dissolution of calcite-rich sediments begins is known as the lysocline, which is a sediment property (Zeebe & Westbroek 2003). The lysocline and CCD serve as bounds on the transition zone (~ 0.5 km) between calcite-rich and calcite-free sediments. Other definitions for the CCD exist (Berger et al. 1976; Ridgwell & Zeebe 2005; Zeebe 2012). The depth of ocean d (km) in terms of ocean pressure P_{oc} (bar) at the equator is given by (Leroy & Parthiot 1998)

$$d = \frac{1}{9.7803 \times 10^3 + 0.011 P_{\text{oc}}} (97.266 P_{\text{oc}} - 2.512 \times 10^{-3} P_{\text{oc}}^2 + 2.28 \times 10^{-7} P_{\text{oc}}^3 - 1.8 \times 10^{-11} P_{\text{oc}}^4). \quad (14)$$

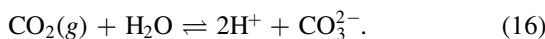
We consider the CCD to be the depth d_{CCD} (equivalent to the ocean pressure where $P_{\text{oc}} = P_{\text{CCD}}$) at which 99.9% of near-surface ($P_{\text{oc}} = P_{\text{surf}}$) Ca, Mg, or Fe carbonates dissolve:

$$n_{\text{Carb,CCD}} = 0.001 n_{\text{Carb,surf}}. \quad (15)$$

Our calculations of CCD are performed up to $d_{\text{CCD}} = 45$ km because of the availability of thermodynamic data up to the pressure of 5000 bar (Zimmer et al. 2016). This limitation does not affect our conclusions.

2.4. Analytical Solution of Ocean pH

Upper limit of ocean pH. For calcite precipitation, all reactions in Section 2 need to be satisfied. However, two of these reactions can be used to analytically constrain ocean pH: Equations (9) and (16), where Equation (16) is a combination of Equations (3) and (5):



The ocean pH can be written as a function of P_{CO_2} , $n_{\text{Ca}^{2+}}$, and equilibrium constants of Equations (9) and (16) (Appendix A):

$$\text{pH} = -\frac{1}{2} \left(\log P_{\text{CO}_2} + \log K_9 K_{16} + \log \frac{n_{\text{Ca}^{2+}}}{n_0} \right). \quad (17)$$

This equation demonstrates the reason for the slope of approximately -0.5 for the upper limit of ocean pH as a function of the logarithm (base 10) of P_{CO_2} . Because K_9 and K_{16} are constants at a fixed T and P , pH becomes a function of only P_{CO_2} and $n_{\text{Ca}^{2+}}$ in Equation (17). As a function of P_{CO_2} , $n_{\text{Ca}^{2+}}$ at the limit of carbonate saturation varies between $\sim 0.1 \text{ m}^{-3}$ (at $P_{\text{CO}_2} = 0.01 \mu\text{bar}$) and $\sim 6 \text{ m}^{-3}$ (at $P_{\text{CO}_2} = 0.3$ bar). This additional increase in $n_{\text{Ca}^{2+}}$ of less than two orders of magnitude over seven orders of magnitude increase in P_{CO_2} makes the slope of ocean pH slightly steeper than -0.5 (see Figure A1). Using $n_{\text{Ca}^{2+}}$ from the numerical solution in Equation (17) results in a semi-analytical solution matching with the numerical solution until $P_{\text{CO}_2} = 0.1$ bar, beyond which nonideal effects accounted in the numerical solution exhibit a small deviation from the analytical equation.

Lower limit of ocean pH. In the absence of divalent cations in ocean, the ocean pH is largely governed by the conversion of CO_2 to protons (Equation (3)). For $P_{\text{CO}_2} > 1 \mu\text{bar}$, the ocean is acidic, where the number density of H^+ is larger than that of OH^- and the number density of HCO_3^- is larger than CO_3^{2-} (bicarbonate-carbonate-water equilibria; Wolf-Gladrow et al. 2007). Therefore, the charge balance equation can be approximated as

$$n_{\text{H}^+} = n_{\text{HCO}_3^-}. \quad (18)$$

In terms of the equilibrium constant of Equation (3), this leads to (Appendix A)

$$\text{pH} = -\frac{1}{2} (\log P_{\text{CO}_2} + \log K_3). \quad (19)$$

At a fixed T and P , K_3 is constant and thus the ocean pH exhibits a slope of -0.5 for $P_{\text{CO}_2} > 1 \mu\text{bar}$ (Figure A1). For $P_{\text{CO}_2} < 1 \mu\text{bar}$, the analytical solution does not hold because the number density of OH^- is significant enough to make the charge balance approximation in Equation (18) invalid. The lower limit of ocean pH is independent of the Ca, Mg, or Fe systems considered.

3. Results and Discussion

We consider the ocean pH to be determined by the chemical dissolution of atmospheric carbon dioxide in a well-mixed ocean, which occurs at the atmosphere–ocean interface. The chemical dissolution of CO_2 is governed by the reaction between water and CO_2 to produce H^+ , HCO_3^- , and CO_3^{2-} ions (Section 2). As P_{CO_2} increases, the ocean becomes more acidic. We consider an atmospheric surface pressure of 1 bar, but allow the atmospheric carbon dioxide content to vary via P_{CO_2} . Atmospheric surface pressures up to 100 bar have a negligible effect on our results and those between 100 and 1000 bar exhibit a small effect (Figure A2(a)).

For a given value of P_{CO_2} , the ocean pH is bounded between two limits (Figure 2(a)). The ocean pH is restricted to a narrow range between 7–11 at $P_{\text{CO}_2} = 0.01 \mu\text{bar}$ and 4–7 for $P_{\text{CO}_2} = 0.1$ bar. These ocean pH ranges are consistent with the inferences for Earth’s history, transitioning from an acidic ocean during the Archean at high P_{CO_2} to an alkaline ocean at the present-day P_{CO_2} (Halevy & Bachan 2017; Krissansen-Totton et al. 2018). The lower limit corresponds to the complete absence of divalent cations and thus it is independent of the carbonate system under investigation (Section 2). The

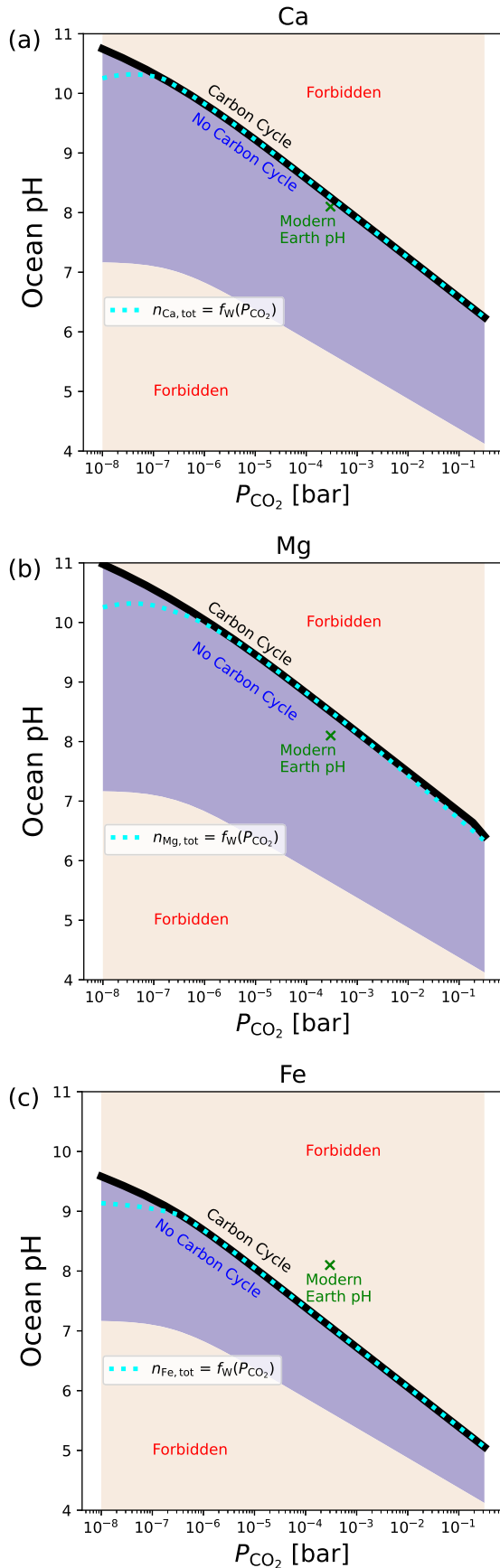


Figure 2. Sensitivity of ocean pH to P_{CO_2} at $T = 288$ K for pure (a) Ca, (b) Mg, and (c) Fe systems. Upper and lower bounds of ocean pH are represented by the blue shaded region. Pink shaded regions are forbidden.

upper limit corresponds to the saturation of calcium cations in ocean water such that more weathering does not produce further changes in pH and simply produces more calcite. This upper limit is buffered by the precipitation of carbonates and hence results in one solution of ocean pH when the carbon cycle is operational for a given carbonate system and P_{CO_2} . Both upper and lower limits of ocean pH follow a slope of approximately -0.5 as a function of P_{CO_2} (see Section 2.4). Between these two limits, the number density of calcium cations is below the threshold to precipitate carbonates onto the ocean floor; thus, the carbon cycle is not operational.

Due to their high condensation temperatures, the relative abundances of refractory elements observed in the photosphere of stars are expected to be mirrored in the rocky exoplanets they host (Bond et al. 2010; Thiabaud et al. 2015). For example, the calcium-to-magnesium ratio of the solar photosphere and Earth are 0.062 and 0.066, respectively (Lodders 2003; Elser et al. 2012). The relative abundances of Ca, Mg, and Fe, measured from the spectra of stars, vary by up to an order of magnitude. For example, $\text{Ca}/\text{Mg} = 0.02\text{--}0.2$ and $\text{Ca}/\text{Fe} = 0.04\text{--}0.2$ in the Hypatia catalog of more than 7000 stars (Hinkel et al. 2014). Furthermore, carbonates involving Mg and Fe are known to have formed during Earth’s history, e.g., magnesite (MgCO_3) and siderite (FeCO_3). These carbonates have dissolution properties that differ from those of calcite. Siderite could have played a key role in locking up CO_2 in carbonates on Earth during the Archean (Rye et al. 1995; Sverjensky & Lee 2010). We calculate ocean pH for the pure Mg and Fe systems in addition to the Ca system (Figures 2(b), (c)). The upper limit of ocean pH for a given P_{CO_2} varies when considering systems with purely Ca, Mg, or Fe as the source of weathering cations. The upper limit of ocean pH for the Mg system is only 0.2 higher than for the Ca system, whereas it is more than unity lower for the Fe system.

For $P_{\text{CO}_2} < 10 \mu\text{bar}$, ocean chemistry is sensitive to the addition of aqueous silica (SiO_2) in the ocean (Figure 3). Silica is another product of silicate weathering, which enables the locking up of cations in silicate minerals instead of carbonate minerals (Walker et al. 1981; Hakim et al. 2021). For instance, for $T > 300$ K and $P_{\text{CO}_2} < 0.1 \mu\text{bar}$ in the Ca system in the presence of aqueous silica, silicates impinge on the stability of calcite (Figure 4(a) and prevent carbonate precipitation at all depths (Figure 3(a)). In contrast, when no silica is present in the ocean for $T > 300$ K and $P_{\text{CO}_2} < 0.1 \mu\text{bar}$, calcite is stable (Figure B2(a)) and deep CCDs are produced (Figure B1(a)), thereby increasing the parameter space where the carbon cycle is stable. Similarly, in the Mg and Fe systems, silicates are more stable than carbonates for $P_{\text{CO}_2} < 10 \mu\text{bar}$ (Figures 4(b), (c)). $P_{\text{CO}_2} > 10 \mu\text{bar}$ favors the thermodynamic stability of carbonates over silicates.

Carbon cycle box models of exoplanets often omit self-consistent modeling of ocean chemistry and precipitation of carbonates. Carbonate precipitation is implicitly assumed to persist and is not expected to be a bottleneck for carbon cycling. Our ocean chemistry model can be incorporated directly into carbon cycle box models for exoplanets, which can couple via key parameters, P_{CO_2} , and the carbonate chemistry. Thermochemical equilibrium calculations of our ocean model can be used to determine the carbon fluxes into or out of the near-surface reservoirs. The carbon cycle box models can also be informed of the effect of ocean chemistry and ocean depth on the efficiency of carbon degassing and recycling.

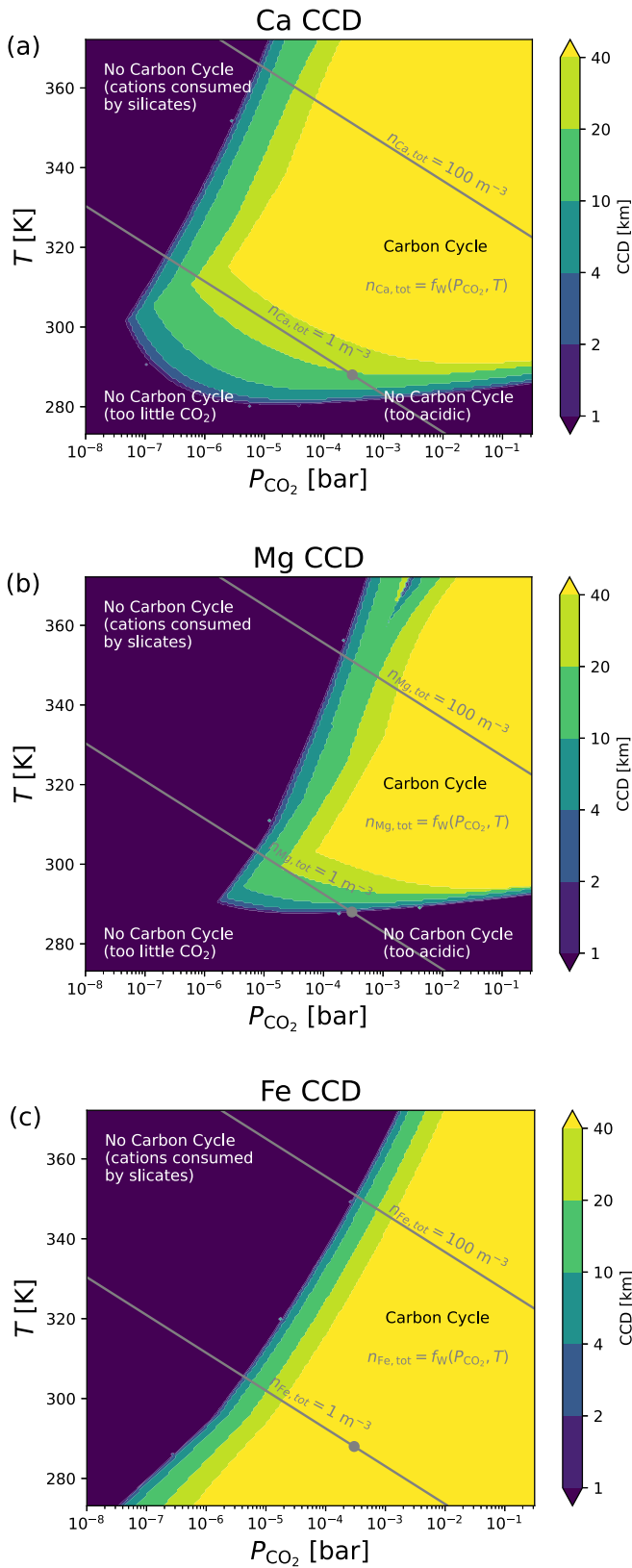


Figure 3. Carbonate compensation depth (CCD) as a function of P_{CO_2} and T ($P_{\text{atm}} = 1$ bar) for (a) Ca, (b) Mg, and (c) Fe systems. Gray contours represent the weathering-dependent cation number density as a function of P_{CO_2} and T (Equation (13)). Gray disk denotes modern Earth P_{CO_2} and T .

Upcoming observations of terrestrial exoplanets from the JWST, ARIEL, and ELTs will put constraints on their atmospheric composition, for instance the volume mixing ratio

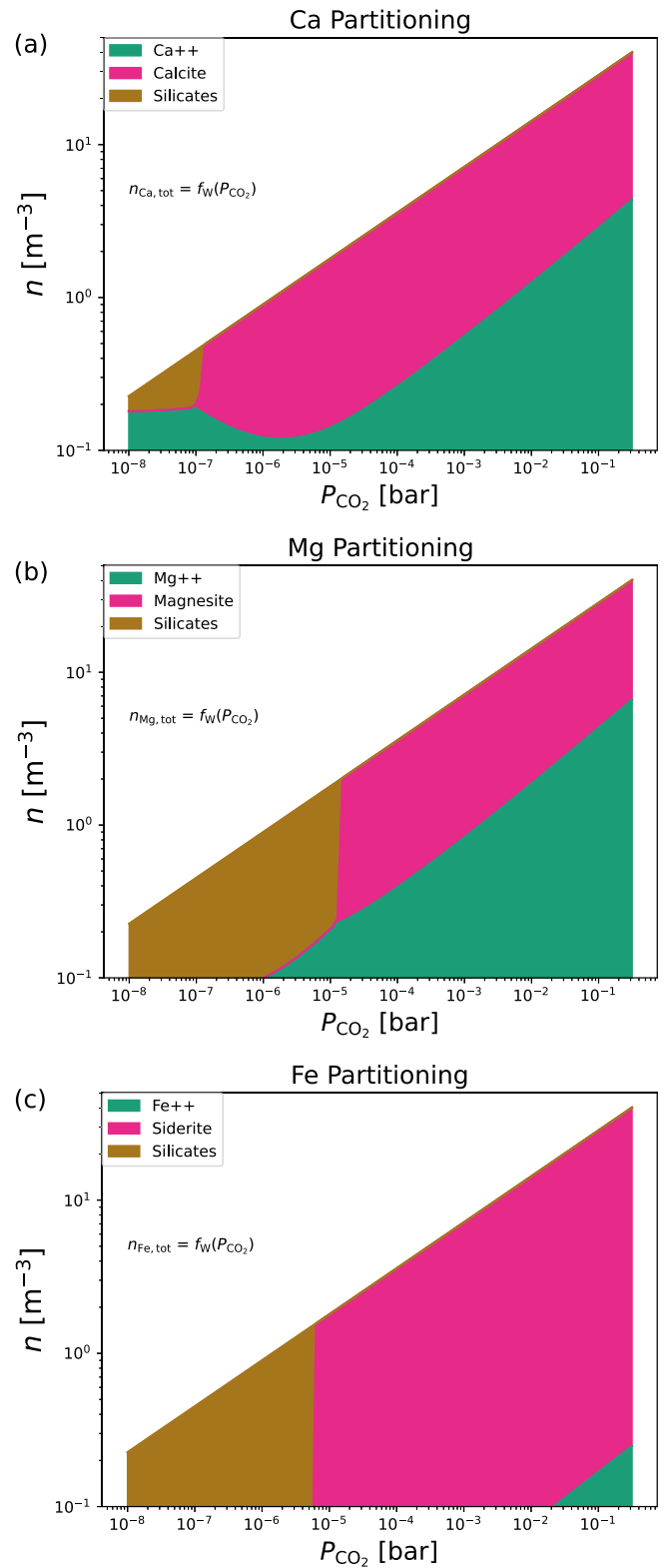


Figure 4. Partitioning of (a) Ca, (b) Mg, and (c) Fe in aqueous, carbonate, and silicate phases as a function of P_{CO_2} at $T = 310$ K ($P_{\text{atm}} = P_{\text{oc}} = 1$ bar) in pure Ca, Mg, and Fe systems, respectively.

of atmospheric carbon dioxide (P_{CO_2}/P). Determining the partial pressure of carbon dioxide (P_{CO_2}) requires the atmospheric surface pressure (P), which is not easily constrained. Nonetheless, our thermodynamic calculations provide strong constraints on ocean chemistry in the presence or absence of

magnesium, calcium or iron carbonates; the relative abundances of these carbonate-forming elements in planetary systems can be deduced from observations of stellar photospheres. Our results suggest that the carbon cycle will operate robustly on chemically diverse terrestrial exoplanets exhibiting silicate weathering. This implies that the search for life from exoplanets with temperate climates or biospheres will benefit by broadening the target list to planets that are more chemically diverse than Earth.

We acknowledge financial support from the European Research Council via Consolidator Grant (ERC-2017-CoG-771620-EXOKLEIN, awarded to K.Heng) and the Center for Space and Habitability, University of Bern. We thank Allan Leal for his support with Reaktoro.

Data availability

All data generated or analyzed during this study are included in the published article.

Code availability

OCRA (Ocean Chemistry with Reaktoro And beyond): the open-source code developed in this work is hosted at <https://github.com/kaustubhhakim/ocra>. OCRA v1.0 was used in this study and is also available on Zenodo (Hakim 2022).

Software: numpy (Harris et al. 2020), scipy (Virtanen et al. 2020), pandas (The pandas development team 2020), astropy (Astropy Collaboration et al. 2013; Astropy Collaboration et al. 2022), matplotlib (Hunter 2007), Reaktoro (Leal 2015).

Appendix A

Analytical Solution of Ocean pH and P – T Sensitivity

The analytical solution for the upper limit of ocean pH is derived from the relations between the equilibrium constants and reactants and products (assuming water activity to be unity in diluted solutions) of reactions described by Equations (9) and (16),

$$K_9 = \frac{n_0^2}{n_{\text{Ca}^{2+}} n_{\text{CO}_3^{2-}}}, \quad (\text{A1})$$

$$K_{16} = \frac{n_{\text{H}^+}^2 n_{\text{CO}_3^{2-}}}{P_{\text{CO}_2} n_0^3}. \quad (\text{A2})$$

By eliminating the carbonate ion number density from these two equations, the proton number density is

$$\frac{n_{\text{H}^+}}{n_0} = \left(P_{\text{CO}_2} K_9 K_{16} \frac{n_{\text{Ca}^{2+}}}{n_0} \right)^{1/2}. \quad (\text{A3})$$

Because the pH is given by

$$\text{pH} = -\log(n_{\text{H}^+}/n_0), \quad (\text{A4})$$

the analytical upper limit of ocean pH is Equation (17).

The analytical solution for the lower limit of ocean pH is derived from the equilibrium constant of the reaction described by Equation (3):

$$K_3 = \frac{n_{\text{H}^+} n_{\text{HCO}_3^-}}{P_{\text{CO}_2} n_0^2}. \quad (\text{A5})$$

Then, the proton number density is

$$\frac{n_{\text{H}^+}}{n_0} = \frac{K_3 P_{\text{CO}_2} n_0}{n_{\text{HCO}_3^-}}. \quad (\text{A6})$$

Thus, the lower limit of ocean pH is given by Equation (19).

The analytical solutions of the upper and lower limits of ocean pH as a function of P_{CO_2} result in a slope of -0.5 (Figure A1). Pressure and temperature have a negligible effect on ocean pH (Figure A2).

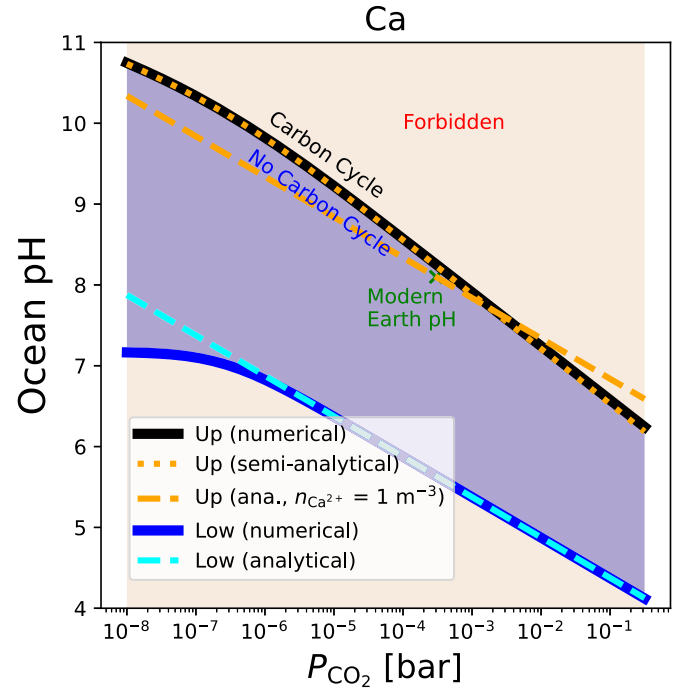


Figure A1. Numerical, analytical, and semi-analytical solutions of the upper and lower limits of ocean pH in the Ca system.

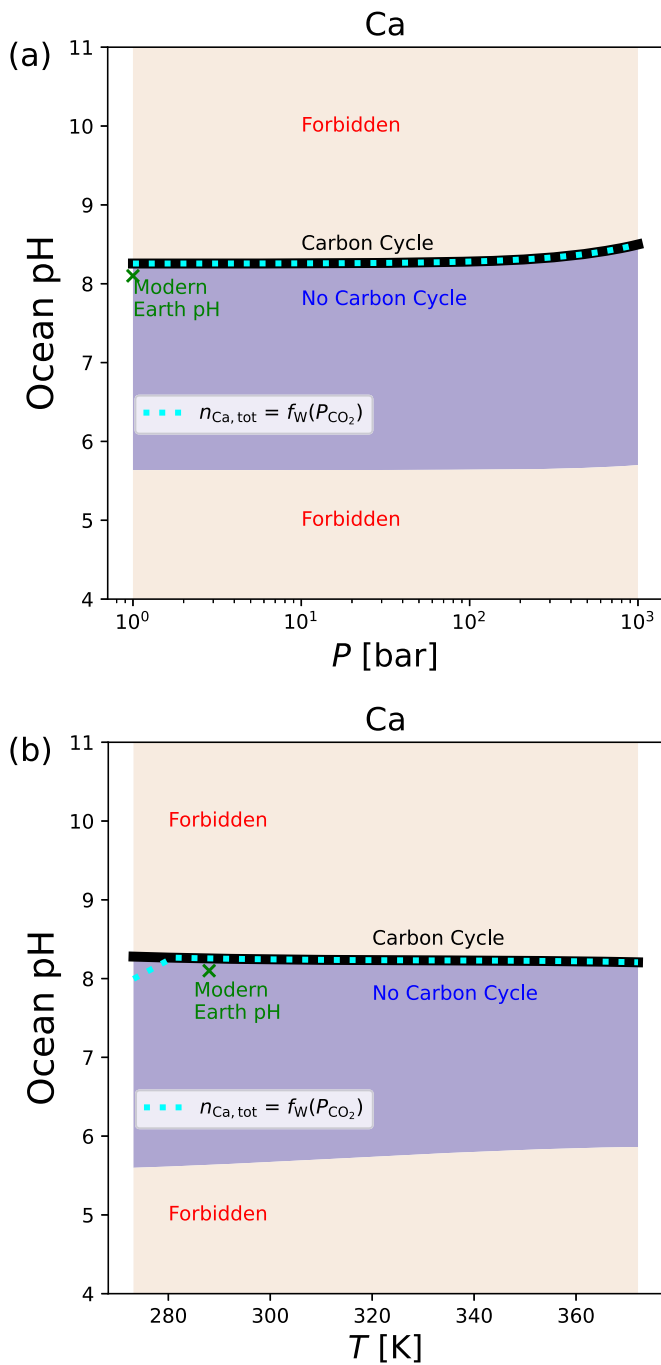


Figure A2. The sensitivity of ocean pH to (a) P and (b) T in the Ca system.

Appendix B Carbonate Compensation Depth without Silicate Precipitation

When no silicates are allowed to precipitate, CCDs for the Ca, Mg, and Fe systems become deeper for $P_{CO_2} < 1 \mu\text{bar}$ (Figure B1). This is reflected in the phase stability plots in Figure B2.

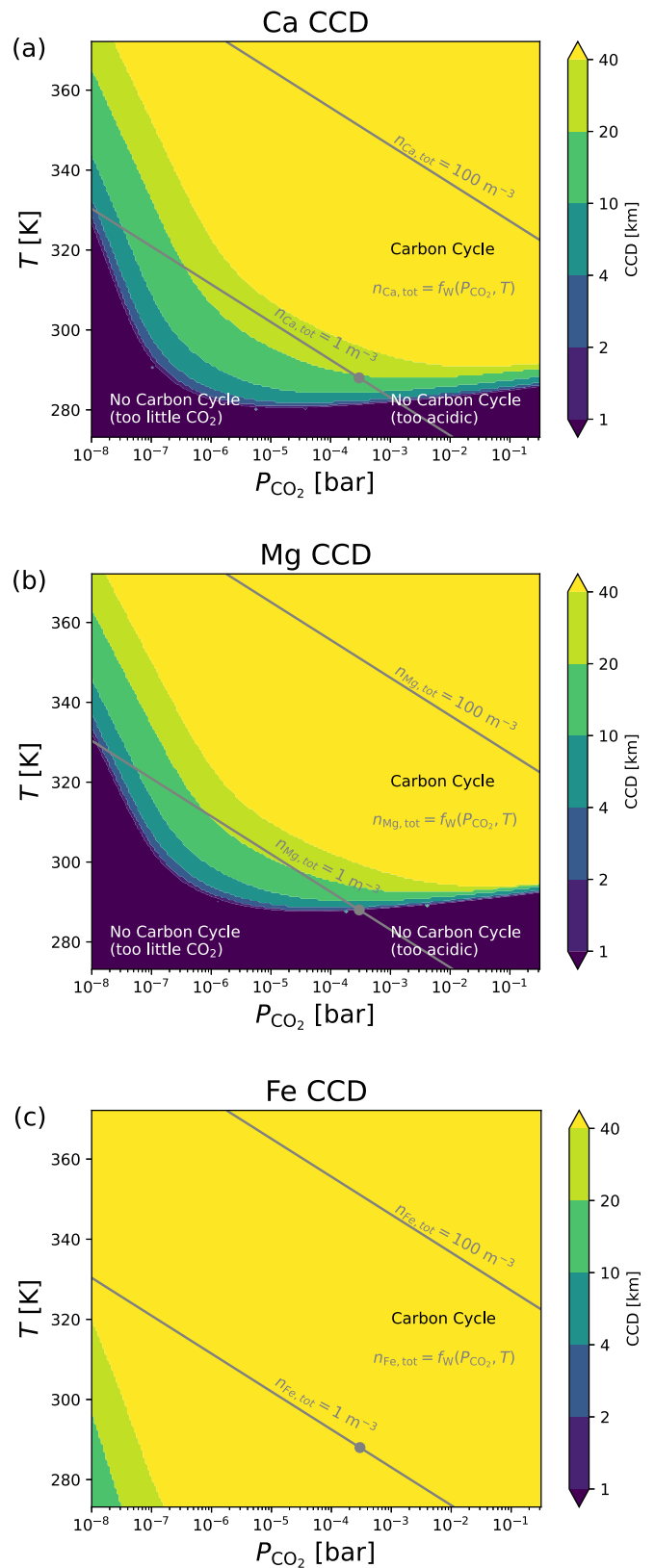


Figure B1. Same as Figure 3 but with no silica $n_{SiO_2,tot} = 0$.

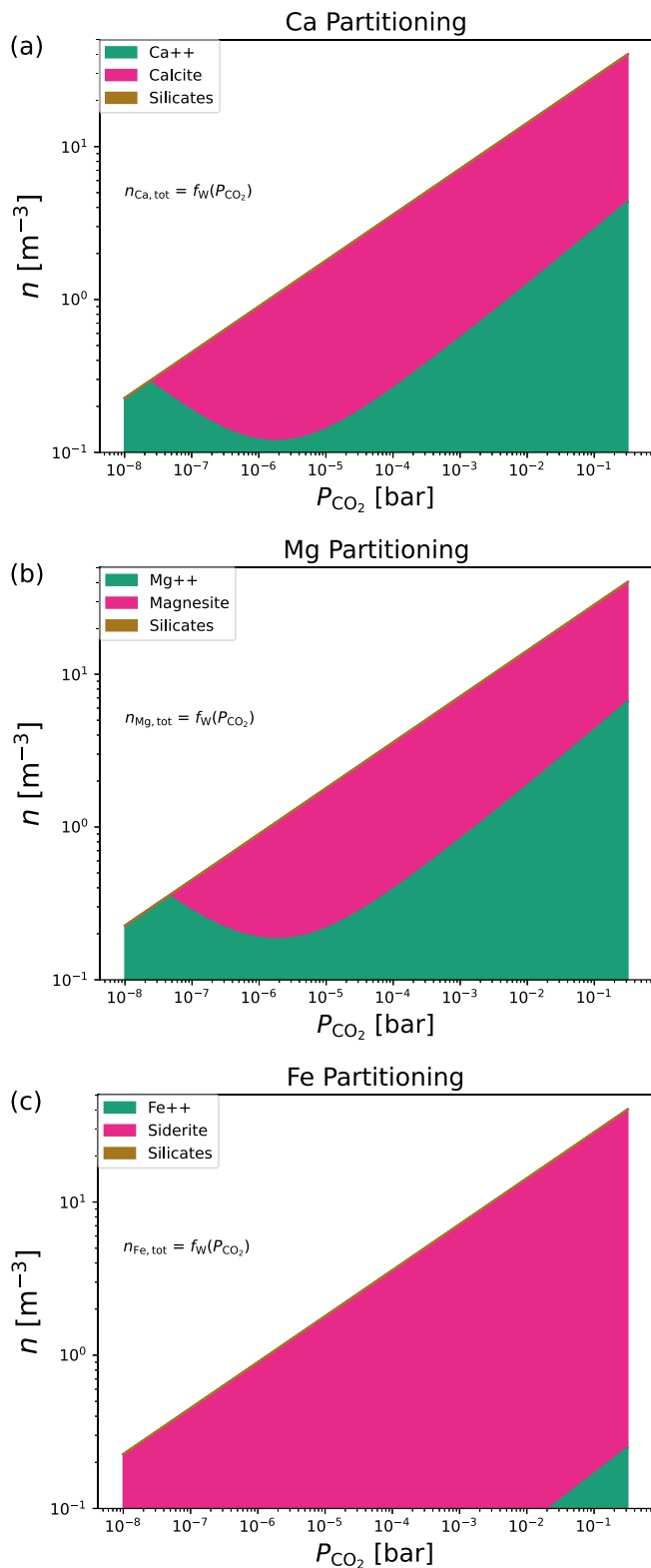


Figure B2. Same as Figure 4 but with no silica $n_{\text{SiO}_2,\text{tot}} = 0$.

ORCID iDs

Kaustubh Hakim  <https://orcid.org/0000-0003-4815-2874>

Meng Tian  <https://orcid.org/0000-0002-7384-8577>

Dan J. Bower  <https://orcid.org/0000-0002-0673-4860>

Kevin Heng  <https://orcid.org/0000-0003-1907-5910>

References

- Astropy Collaboration, Price-Whelan, A. M., Lim, P. L., et al. 2022, *ApJ*, **935**, 167
- Astropy Collaboration, Robitaille, T. P., Tollerud, E. J., et al. 2013, *A&A*, **558**, A33
- Berger, W. H., Adelseck, C. G., & Mayer, L. A. 1976, *JGR*, **81**, 2617
- Berner, R. A. 2004, *The Phanerozoic Carbon Cycle: CO₂ and O₂* (Oxford: Oxford Univ. Press)
- Bond, J. C., O'Brien, D. P., & Lauretta, D. S. 2010, *ApJ*, **715**, 1050
- Catling, D. C., & Kasting, J. F. 2017, *Atmospheric Evolution on Inhabited and Lifeless Worlds* (Cambridge: Cambridge Univ. Press)
- Drummond, S. 1981, PhD thesis, Pennsylvania State University
- Elser, S., Meyer, M. R., & Moore, B. 2012, *Icar*, **221**, 859
- Foley, B. J. 2015, *ApJ*, **812**, 36
- Hakim, K. 2022, kaustubhhakim/ocra: OCRA, v1.0, Zenodo, doi:10.5281/zenodo.7380526
- Hakim, K., Bower, D. J., Tian, M., et al. 2021, *PSJ*, **2**, 49
- Halevy, I., & Bachan, A. 2017, *Sci*, **355**, 1069
- Harris, C. R., Millman, K. J., van der Walt, S. J., et al. 2020, *Natur*, **585**, 357
- Helgeson, H. C., Kirkham, D. H., & Flowers, G. C. 1981, *AmJS*, **281**, 1249
- Hinkel, N. R., Timmes, F. X., Young, P. A., Pagano, M. D., & Turnbull, M. C. 2014, *AJ*, **148**, 54
- Holland, H. D. 1978, *The chemistry of the atmosphere and oceans* (New York: Wiley-Interscience)
- Hunter, J. D. 2007, *CSE*, **9**, 90
- Johnson, J. W., Oelkers, E. H., & Helgeson, H. C. 1992, *CG*, **18**, 899
- Kasting, J. F., Whitmire, D. P., & Reynolds, R. T. 1993, *Icar*, **101**, 108
- Kelemen, P. B., & Manning, C. E. 2015, *PNAS*, **112**, E3997
- Krissansen-Totton, J., Arney, G. N., & Catling, D. C. 2018, *PNAS*, **115**, 4105
- Leal, A. M. M. 2015, *Reaktoro: An Open-source Unified Framework for Modeling Chemically Reactive Systems*, v1, <https://reaktoro.org>
- Leal, A. M. M., Kulik, D. A., Smith, W. R., & Saar, M. O. 2017, *PApCh*, **89**, 597
- Leroy, C. C., & Parthiot, F. 1998, *ASAJ*, **103**, 1346
- Lodders, K. 2003, *ApJ*, **591**, 1220
- Peng, D.-Y., & Robinson, D. B. 1976, *Ind. Eng. Chem.*, **15**, 59
- Ridgwell, A., & Zeebe, R. 2005, *E&PSL*, **234**, 299
- Rye, R., Kuo, P. H., & Holland, H. D. 1995, *Natur*, **378**, 603
- Sleep, N. H., & Zahnle, K. 2001, *JGR*, **106**, 1373
- Sverjensky, D. A., & Lee, N. 2010, *Elem*, **6**, 31
- The pandas development team 2020, pandas-dev/pandas: Pandas 1.0.0 Zenodo, doi:10.5281/zenodo.3509134
- Thiabaud, A., Marboeuf, U., Alibert, Y., Leya, I., & Mezger, K. 2015, *A&A*, **580**, A30
- Virtanen, P., Gommers, R., Oliphant, T. E., et al. 2020, *NatMe*, **17**, 261
- Walker, J. C. G., Hays, P. B., & Kasting, J. F. 1981, *JGR*, **86**, 9776
- Wolf-Gladrow, D. A., Zeebe, R. E., Klaas, C., Kortzinger, A., & Dickson, A. G. 2007, *MarCh*, **106**, 287
- Zeebe, R. E. 2012, *AREPS*, **40**, 141
- Zeebe, R. E., & Westbroek, P. 2003, *GGG*, **4**, 1104
- Zimmer, K., Zhang, Y., Lu, P., et al. 2016, *CG*, **90**, 97